JOURNAL OF AGRICULTURAL AND FOOD CHEMISTRY

Agricultural and Environmental Chemistry

Synthesis of Thiazolium-Labeled 1,3,4-Oxadiazole Thioethers as Prospective Antimicrobials: In Vitro and In Vivo Bioactivity and Mechanism of Action

Ming-Wei Wang, Huai-He Zhu, Peiyi Wang, Dan Zeng, Yuan-Yuan Wu, Li-Wei Liu, Zhibing Wu, Zhong Li, and Song Yang

J. Agric. Food Chem., **Just Accepted Manuscript** • DOI: 10.1021/acs.jafc.9b03952 • Publication Date (Web): 28 Oct 2019

is published by the American Chemical Society. 1155 Sixteenth Street N.W., Washington, DC 20036

Synthesis of Thiazolium-Labeled 1,3,4-Oxadiazole Thioethers as Prospective Antimicrobials: In Vitro and In Vivo Bioactivity and Mechanism of Action

Ming-Wei Wang [†] [a], Huai-He Zhu [†] [a], Pei-Yi Wang* [a], Dan Zeng [a], Yuan-Yuan Wu [a], Li-Wei Liu [a], Zhi-Bing Wu [a], Zhong Li [b], Song Yang* [a,b]

[a] State Key Laboratory Breeding Base of Green Pesticide and Agricultural Bioengineering, Key Laboratory of Green Pesticide and Agricultural Bioengineering, Ministry of Education, Center for R&D of Fine Chemicals of Guizhou University, Guiyang, 550025, China.

[b] College of Pharmacy, East China University of Science & Technology, Shanghai, China 200237.

* Corresponding author.

E-mail: jhzx.msm@gmail.com (S. Yang), pywang888@126.com (P.-Y. Wang)

[†] The two authors contribute equally to this work.

Abstract

In this study, a type of thiazolium-labeled 1,3,4-oxadiazole thioether bridged by diverse alkyl chain lengths was constructed. The antimicrobial activity of the fabricated thioether towards plant pathogenic bacteria and fungi was then screened. Antibacterial evaluation indicated that title compounds possess specific characteristics that enable it to severely attack three phytopathogens, namely, *Xanthomonas oryzae pv. oryzae*, *Ralstonia solanacearum*, and *Xanthomonas axonopodis pv. citri* with minimal EC_{50} of 0.10, 3.27, and 3.50 μg/mL, respectively. Three-dimensional quantitative structure–activity relationship models were established to direct the following excogitation for exploring higher active drugs. The in vivo study against plant bacterial diseases further identified the prospective application of title compounds as alternative antibacterial agents. The proteomic technique, scanning electron microscopy patterns, and fluorescence spectrometry were exploited to investigate the antibacterial mechanism. Additionally, some target compounds performed superior inhibitory actions against three tested fungal strains. In view of their simple molecular architecture and highly efficient bioactivity, these substrates could be further explored as promising surrogates for fighting against plant microbial infections.

Keywords

1,3,4-oxadiazole, thiazolium, antimicrobial, 3D-QSAR, proteomics, action mechanism

39

40 **1. Introduction**

41 Despite the remarkable contribution of commercial antibiotic therapies to agriculture
42 in the past decade,[1-2] microbial infections continue to cause global agricultural
43 production constraints because of the poor efficiency of existing commercial
44 antibiotic agents toward invasive phytopathogens and the emergence of a growing
45 number of multidrug-resistant microorganisms originating from various factors, such
46 as long-term usage of traditional bactericides bearing a single mode of action.[3-7] In
47 addition, evidence shows that a large-scale outbreak of resistance can rapidly
48 accelerate within a relatively short period once resistant pathogenic races appear; this
49 condition further exacerbates the difficulty in managing this serious issue and elevates
50 the potential risks on human health.[8-11] Thus, innovative structures to develop simple
51 and highly efficient antimicrobial drugs possessing unique modes of actions are better
52 alternatives to analogues of existing ones for the treatment of plant bacterial or fungal
53 diseases.

54 In drug design programs, one of the most efficient and promising approaches to
55 explore securely bioactive structures is based on existing pharmacological skeletons
56 from naturally occurring products, which have been verified to have a variety of
57 advantages, including inartificial structural features, well-balanced physicochemical
58 property, good biocompatibility, permissible environmental friendliness, low
59 cytotoxicity toward mammalian cells, and unique modes of action.[12-17] Among these
60 native structural fragments, the thiazolium scaffold has been elaborately explored and

61 highlighted because it is a crucially active component of thiamine (vitamin B_1) and
62 thiamin pyrophosphate (ThDP) and serves as a cofactor of certain enzymes or
63 multi-enzyme complexes, including pyruvate decarboxylase, α-ketoglutarate
64 dehydrogenase and transketolase, catalyzing several biochemical reactions in all
65 living organisms; in addition, this favorable building block offers diverse capabilities
66 in various aspects, such as improving the balance of the physicochemical and
67 amphiphilic properties of target molecules, allowing decoration with functional
68 groups, and reforming molecular pharmacological activities.[18-20] Thus, comprehensive
69 investigations into this flexible motif are still being conducted, resulting in an array of
70 thiazolium-tailored compounds with excellent potential applications (Figure 1). For
71 instance, furazolium chloride containing a thiazolium moiety was discovered and
72 developed as a powerful antimicrobial agent against *Proteus vulgaris*, *Pseudomonas*
73 *aeruginosa*, *Salmonella typhosa*, and *Staphylococcus aureus*.[21] Meanwhile, Kim et
74 al.[22] evaluated the antibacterial effects of a type of cephalosporin derivative carrying a
75 thiazolium motif and found that these designed molecules exhibited potent
76 bioactivities against Gram-positive and Gram-negative microorganisms except *P.*
77 *aeruginosa*. In addition, three highly bioactive structures bearing bis-thiazolium
78 patterns exhibited in vitro antimalarial activities against the protozoan parasite
79 *Plasmodium falciparum* with IC_{50} values of 2.6 (R = $-CH_2OH$), 0.7 (R = $-CH_2OCH_3$),
80 and 25.0 nM (R = $-CH_3$); (R = $-CH_2OH$) is currently being clinically investigated by
81 Sanofi–Aventis and has entered phase II clinical trials on account of the promising
82 results in vivo study.[23-25] Inspired by these results, the integration of a thiazolium

83 motif in a target molecule may lead to improved biological activities for its versatile
84 functions of this valuable moiety.

85 Meanwhile, 1,3,4-oxadiazole skeleton that acts as another versatile building
86 block has been extensively studied and developed for its dramatic behavior in
87 reforming the bioactivity.[26-30] It can serve as a desirable surrogate for carboxylic
88 acids, esters, and amides, which are always accompanied by augmented biological
89 silhouettes.[31-33] A certain amount of designed frameworks owning 1,3,4-oxadiazole
90 moieties are in the commercialization stage or have been launched into the market.
91 For example, zibotentan[34] (anticancer agent) and furamizole[35] (antibiotic agent) are in
92 the late stage of clinical trials, whereas raltegravir[36] and fenadiazole[37] that serve as
93 antiretroviral and hypnotic drugs, respectively, have been successfully exploited to
94 manage HIV infection and insomnia. In our previous works, we demonstrated that
95 1,3,4-oxadiazole thioether/sulfoxide/sulfone derivatives possess superior bioactivities
96 against plant bacterial diseases; two sulfone candidates (5-(4-fluorophenyl or
97 2,4-dichlorophenyl)-2-(methylsulfonyl)-1,3,4-oxadiazole) are in the novel pesticide
98 registration stage.[33,38] Such diverse range of applications motivates us to explore and
99 develop 1,3,4-oxadiazole-labeled derivatives as prospective antimicrobial surrogates.

100 As another key fragment, the silhouette of 2,4-dichlorophenyl is always
101 observable in existing pesticide chemicals,[39-41] especially for antibiotic structures such
102 as triarimole, diniconazole, and hexaconazole.[42,43] Therefore, the fusion of these
103 bioactive substructures of thiazolium, 1,3,4-oxadiazole, and 2,4-dichlorophenyl in a
104 single molecule may probably promote the discovery of excellent substrates as

105 antimicrobial indicators against plant microbial diseases (Figure 2). In our previous
106 works, we have evaluated the antibacterial functions of various pyridinium-tailored
107 derivatives.[44,45] However, pyridinium-tailored derivatives displayed significant
108 phytotoxicity (Figure S1a-S1b, supporting information). To explore novel frameworks
109 with low phytotoxicity and highly efficient antimicrobial ability, herein, a series of
110 5-(2,4-dichlorophenyl)-1,3,4-oxadiazole thioethers bearing natural thiazolium
111 scaffolds linked by different alkyl chain lengths[46,47] was initially fabricated. The
112 antimicrobial effects of these thioethers against three invasive and widespread
113 phytopathogens, namely, *Xanthomonas oryzae pv. oryzae* (*Xoo*), *Ralstonia*
114 *solanacearum* (*R. solanacearum*), and *Xanthomonas axonopodis pv. citri* (*Xac*); as
115 well as three virulent phytopathogenic fungi, namely, including *Gibberella zeae* (*G.*
116 *zeae*), *Fusarium oxysporum* (*F. oxysporum*), and *Phytophthora cinnamomi* (*P.*
117 *cinnamomi*), were evaluated. Subsequently, the substituents at the 5-position of
118 1,3,4-oxadiazole toward bioactivity were also investigated. On the basis of the
119 obtained molecular structures and collected bioassay data, three-dimensional
120 quantitative structure–activity relationship (3D-QSAR) models were established to
121 direct the following excogitation for exploring higher active drugs. An in vivo study
122 against plant bacterial diseases was performed to identify the prospective application
123 of these compounds as alternative antibacterial agents. Meanwhile, the proteomic
124 technique, scanning electron microscopy (SEM), and fluorescence spectrometry were
125 exploited to investigate the antimicrobial mechanism of the thioethers.

126 **2. Materials and methods**

127 **2.1 Instruments and Chemicals**

128 Instruments: NMR, JEOL-ECX-500 and Bruker Biospin AG-400 apparatuses;
129 Centrifuge, Centrifuge 5424 R, eppendorf; spectrometer (UV-Vis), Fluoromax-4
130 Spectrofluorometer, HORIBA Scientific; High resolution mass spectrometer,
131 UItiMate 3000, Thermo SCIENTIFIC; Melting point apparatus, SGW® X-4B,
132 Shanghai Yidian Physical Optical Instrument Co., Ltd; High performance liquid
133 chromatography (HPLC), 1290 Infinity Ⅱ, Agilent Technologies; Scanning electron
134 microscope, FEI Nova NanoSEM 450. All the chemicals (⩾98%) used for reaction
135 were purchased from Energy Chemical of Saen Chemical Technology (Shanghai) Co.,
136 Ltd. The solvents including Ethyl acetate (99.5%), Dichloromethane (99.5%),
137 Methanol (99.5%), Petroleum ether (99.5%), *N,N*-Dimethylformamide (99.5%) and
138 Acetonitrile (AR) were purchased from Tianjin Fuyu Chemical Co., Ltd; Glucose (⩾
139 99.5%) and Beef Extract (Reagent Grade) were purchased from Sangon Biotech
140 (Shanghai) Co., Ltd; Peptone (test reagent LR) was purchased from Shanghai
141 Bio-way technology Co., Ltd; Yeast extract (AR) was purchased from Beijing
142 Solarbio Science & Technology Co., Ltd.

143 **2.2 Experimental section**

144 *In vitro* and *in vivo* antibacterial testing, *in vitro* antifungal testing, label-free
145 quantitative proteomics analysis, PI uptake assay, scanning electron microscopy
146 (SEM), synthesis for intermediates and title compounds, see supplementary data.

147 **3. Results and Discussion**

148 To explore the integration of key fragments of thiazolium, 1,3,4-oxadiazole, and

149 2,4-dichlorophenyl toward bioactivity, we initially constructed thiazolium-tailored
150 5-(2,4-dichlorophenyl)-1,3,4-oxadiazole thioethers bridged by diverse alkyl chain
151 lengths (Figure 3). Intermediate **4** owning a 1,3,4-oxadiazole pattern was obatined as
152 described in our previous approach,[2] which was carried out via two-step reactions
153 with dibromo-substituted alkyls and thiazole (or 4-methylthiazole) to obtain the target
154 compounds $\mathbf{A_n}$ and $\mathbf{B_n}$. The achieved molecules were screened to test their
155 antibacterial potency against *Xoo*, *R. solanacearum*, and *Xac* through a turbidimeter
156 test.[48] The agricultural antibiotic agents thiodiazole copper (**TC**) and bismerthiazol
157 (**BT**) were co-assayed as reference drugs. The screening results (Table 1) revealed
158 that these reconstructed compounds displayed good to excellent antibacterial
159 efficiency against the three tested strains and were relatively superior to **BT** and **TC**.
160 The title compounds exerted selectivity and specificity against *Xoo* with EC_{50} within
161 4.84 μg/mL to 0.23 μg/mL. Notably, the antibiotic competence increased from $\mathbf{A_6}$ to
162 $\mathbf{A_{12}}$ and $\mathbf{B_6}$ to $\mathbf{B_{12}}$ with prolonging alkyl chain lengths, thereby suggesting that the
163 increment of molecular hydrophobicity was beneficial to the bioactivity. In
164 comparison with the substituent group and its thiazolium pattern toward bioactivity,
165 the methyl group displayed a slightly ameliorative tendency, as illustrated by $\mathbf{A_6}$ (4.84
166 μg/mL) < $\mathbf{B_6}$ (3.12 μg/mL), $\mathbf{A_8}$ (3.04 μg/mL) < $\mathbf{B_8}$ (1.87 μg/mL), and $\mathbf{A_{12}}$ (0.24
167 μg/mL) < $\mathbf{B_{12}}$ (0.23 μg/mL). For anti-*R. solanacearum* and anti-*Xac* activities, a
168 plausible posture was observed: the inhibition effect initially increased and then
169 decreased with the fine-tuning of the length of alkyl tailors. Thus, compounds $\mathbf{A_8}$
170 (25.51 and 4.78 μg/mL) and $\mathbf{B_8}$ (29.80 and 3.80 μg/mL) exerted the most laudable

171 antibacterial performance. These findings indicate that compounds $\mathbf{A_{12}}$ and $\mathbf{B_{12}}$
172 exhibited exclusive and promising potency against *Xoo*. Therefore, further
173 optimization and manipulation of the molecular structures were carried out.

174 As compounds $\mathbf{A_{12}}$ and $\mathbf{B_{12}}$ showed excellent potential as antibacterial indicators,
175 the substituents at 5-postion of 1,3,4-oxadiazole toward bioactivity were investigated.
176 Thiazolium-tailored 1,3,4-oxadiazole thioethers with various substitutional units at the
177 5-position and a providential dodecyl tail were synthesized accordingly (Figure 4). In
178 general, these target compounds $\mathbf{C_n}$ and $\mathbf{D_n}$ (n = 1–10) were fabricated following the
179 synthetic protocols of $\mathbf{A_n}$, in which the key intermediate
180 5-(2,4-dichlorophenyl)-1,3,4-oxadiazole-2-thiol was changed into an array of
181 5-substituted-1,3,4-oxadiazole-2-thiol. The obtained structures were characterized by
182 NMR, HRMS, and HPLC (supporting information). The crystal structures of
183 compound $\mathbf{D_7}$ further confirmed the accurate molecular frameworks (Figure 5). A
184 squint in the screening result (Table 2) suggested that this type of compound did
185 possess specific and selective competences for severely attacking pathogen *Xoo* and
186 provided EC_{50} within 0.10 μg/mL to 1.68 μg/mL for compounds $\mathbf{C_n}$ and $\mathbf{D_n}$ (n = 1–
187 10), indicating that the integration of these valuable building blocks could promote
188 the discovery of highly efficient surrogates. The antibacterial efficacy (for compounds
189 $\mathbf{C_1}$ and $\mathbf{D_1}$) was almost maintained after removing the 4-Cl from compounds $\mathbf{A_{12}}$ and
190 $\mathbf{B_{12}}$, whereas the antibiotic capacity (for compounds $\mathbf{C_2}$ and $\mathbf{D_2}$) declined by twofold
191 after the replacement of 2,4-diCl into 4-Cl. Hence, 4-Cl on the benzene ring was
192 slightly negative toward anti-*Xoo* activity. Further breaking the molecular rigidity and

193 introducing a methylene group between the benzene motif and 1,3,4-oxadiazole (for
194 compounds **C_3** and **D_3**) still did not improve the inhibitory effect in comparison with
195 that for compounds **C_2** and **D_2**. The electron-withdrawing groups had an insignificant
196 influence on bioactivity, as indicated by comparing EC_{50} values of **D_5** (4-CF_3, 0.33
197 μg/mL) and **D_6** (4-NO_2, 0.34 μg/mL). Ameliorative antibacterial ability was observed
198 by introducing a methyl group at the 2-position of benzene ring and led to EC_{50} of
199 0.15 and 0.13 μg/mL for compounds **D_8** and **C_8**, respectively. A superior antibacterial
200 candidate (**C_{10}**) bearing 4-fluoro-3-methylphenyl at 5-position of 1,3,4-oxadiazole
201 was discovered with EC_{50} of 0.10 μg/mL. For anti-*R. solanacearum* activity, the
202 antibiotic potency was dramatically elevated by approximately ninefold after
203 changing 2,4-diCl and substituting it into 2-Cl on the benzene ring. Thus, the EC_{50}
204 values varied from 79.71 μg/mL (**A_{12}**) to 8.45 μg/mL (**C_1**) and from 31.28 μg/mL (**B_{12}**)
205 to 3.27 μg/mL (**D_1**). This result suggested that 4-Cl on the benzene ring might block
206 other interactions with bacterial receptors. An opposite pattern for the inhibitory effect
207 was observed after shifting the chlorine atom to the 4-position of the benzene ring (**C_2**,
208 21.72 μg/mL; **D_2**, 11.37 μg/mL). Such observation revealed that the location of the
209 substituents had a significant action toward bioactivity. Notably, the pharmaceutical
210 effect was gravely knocked down after inserting a methylene group (**C_3** and **D_3**) to
211 break the planar pattern of the benzene ring and 1,3,4-oxadiazole core in comparison
212 with those of compounds **C_2** and **D_2**. Compound **C_5** bearing a 4-CF_3 group (39.94
213 μg/mL) showed better activity than that of compound **C_6** owning a 4-NO_2 group
214 (85.27 μg/mL). However, opposite results were obtained for compounds **D_5** and **D_6**

215 with EC_{50} of 43.89 and 7.59 μg/mL, respectively. Hence, the type of
216 electron-withdrawing groups also played a crucial role in judging the final activity of
217 a molecule. Compounds **D_8–D_{10}** possessing electron-donating groups (2-CH_3, 3-OCH_3,
218 4-F-3-CH_3) presented agreeable powers against *R. solanacearum* with EC_{50} of 6.66,
219 7.39, and 6.38 μg/mL, respectively. As for the screening results, compound **C_n**
220 bearing the thiazolium moiety exerted lower antibacterial performance than
221 compound **D_n** owning 4-methylthiazol-3-ium parts; however, compound **C_5**
222 performed slightly better than **D_5**. In terms of anti-*Xac* activity, all compounds exerted
223 acceptable activities with EC_{50} within 3.50 μg/mL to 17.21 μg/mL. Compound **D_7**
224 without any substitutional group on the benzene ring displayed the strongest bacterial
225 growth inhibition effect. This type of compound clearly possessed comprehensive
226 inhibitory actions against the tested bacterial strains, particularly for the pathogen *Xoo*.
227 Hence, the fusion of these favorable fragments of thiazolium and 1,3,4-oxadiazole in
228 a molecule could yield highly efficient antimicrobial alternatives.

229 As these compounds demonstrated powerful antibacterial potentials and
230 promising applications for developing anti-*Xoo* drugs, 3D-QSAR models employing
231 comparative molecular field analysis (CoMFA) and comparative molecular similarity
232 index analysis (CoMSIA) were established to elaborately expound the structure–
233 activity relationship and direct the future excogitation of the molecular structure. By
234 using SYBYL-X 2.0 software, we systematically assembled the 3D structures of 28
235 molecules with the "Sketch Molecule" function and then aligned them on the basis of
236 the common substructure and conformation of compound **C_{10}**, which exhibited the

237 greatest antibacterial potency toward *Xoo*. The alignment pattern is shown in Figure 6.
238 To fabricate the 3D-QSAR models, we denoted the antibacterial activity of all the
239 target compounds as pEC_{50} (Table 3). Twenty of the target molecules were selected as
240 the training set for CoMFA and CoMSIA, while the left molecules were employed as
241 the testing set. The predicted pEC_{50} of all the molecules are listed in Table 3. The
242 predicted results were similar to the corresponding experimental data. The
243 observation of linear correlations for the experimental and predicted pEC_{50} in CoMFA
244 and CoMSIA models manifested the credibly predictive competence of these models
245 (Figure 7). The obtained statistical parameters are illustrated in Table 4. The internal
246 validations of the cross-validated q^2 value (> 0.5) and non-cross-validated coefficient
247 r^2 value (> 0.8) are normally considered as a reference for the predictive capacity of
248 3D-QSAR models. The corresponding q^2 and r^2 values for the CoMFA and CoMSIA
249 models were (0.766, 0.951) and (0.792, 0.976), respectively, thereby satisfying the
250 performance demands. Moreover, the related standard errors of estimate (SEEs) and
251 F-values were (0.123, 54.632) and (0.098, 54.786), respectively. In the CoMFA
252 model, the contributions for steric and electrostatic fields were 59.0 and 41.0%,
253 respectively, indicating that the bioactivity slightly depended on the steric
254 interactions. In the CoMSIA model, the steric, electrostatic, hydrophobic, H-bond
255 donor, and H-bond acceptor contributions were 13.5%, 52.7%, 33.3%, 0.0%, and
256 0.5%, respectively, indicating that electrostatic interactions contributed significantly
257 to the anti-*Xoo* activity. The fabricated contour maps for the CoMFA models were
258 dispalyed in Figure 8. The yellow contours around the benzene ring and thiazolium

259 scaffold in the CoMFA steric field suggested that the large groups at these positions
260 were unfavorable for the bioactivity (Figure 8A), illustrated by comparing EC_{50} of **C_4**
261 (4-F, 0.28 μg/mL) and **C_5** (4-CF_3, 0.39 μg/mL), **C_9** (thiazolium, 0.15 μg/mL) and **D_9**
262 (4-methylthiazol-3-ium, 0.45 μg/mL) bearing the large groups for the latters,
263 respectively. For the CoMFA electrostatic field (Figure 8B), red polyhedra with
264 electron-donating groups increased the activity, displaying by the screening results of
265 compounds **C_9** (3-OCH_3, 0.15 μg/mL), **C_7** (H, 0.44 μg/mL), **D_9** (3-OCH_3, 0.45
266 μg/mL), and **D_7** (H, 1.68 μg/mL). By contrast, the blue pattern with
267 electron-withdrawing groups at this area enhanced the bioactivity in accordance with
268 the observation of a blue color surrounding the thiazolium skeleton. Thus, this
269 fragment was indeed devoted to the bioactivity. The CoMSIA contour maps are
270 presented in Figure 9. The steric field pattern (Figure 9A) revealed that the bulky
271 groups at the 3-position of the benzene ring located at the green region could improve
272 the antibacterial power, as revealed by comparing EC_{50} of **C_{10}** (4-F-3-CH_3, 0.10
273 μg/mL) and **C_4** (4-F, 0.28 μg/mL). For the electrostatic field map (Figure 9B), the
274 blue area suggested that the introduction of electron-withdrawing groups improved
275 the bioactivity, which further verified the strong electron-withdrawing nature of the
276 thiazolium scaffolds powerfully contributing to the antibacterial competence. On the
277 contrary, the red portion located at the 2-position indicated that an electron-donating
278 group was preferred for the bioactivity, as verified from the bioassay result of
279 compounds **C_8** (2-CH_3, 0.15 μg/mL) and **C_1** (2-Cl, 0.20 μg/mL). The hydrophobic
280 field pattern (Figure 9C) showed that integrating the hydrophobic group at the yellow

region or the hydrophilic group at the gray contour would enhance the bioactivity. A red pattern was observed from the H-bond acceptor field map (Figure 9D), and it suggested that the reception of hydrogen bonding in this area could ameliorate the antibacterial efficiency. Given the study's results and structural insights, this model provides an insight for the rational design of fresh bioactive compounds as antibacterial surrogates.

In vivo trials against bacterial blight on rice were performed to identify the prospective application of the developed compounds as agricultural agents. As illustrated in Table 5, Figure 10 and Figure S1c-S1d, the highly active compound $\mathbf{C_{10}}$ presented excellent in vivo curative activity with low phytotoxicity, providing a control efficiency of 48.5% at 200 μg/mL; these results were relatively superior to **BT** (32.8%) and **TC** (39.2%). This compound's protection effect was also remarkable and provided a relevant control rate of 51.5%. This outcome manifested that the designed molecules were capable of fighting against plant bacterial diseases.

To understand the regulatory role and antibacterial mechanism triggered by the thiazolium-labeled 1,3,4-oxadiazole thioethers, we derived a label-free quantitative proteomic profile by treating *Xoo* with hyperactive compound $\mathbf{C_{10}}$. The quality of the obtained result was assessed and confirmed from Figure S2. Meanwhile, the enriched peptides were monitored by LC–MS/MS and were subsequently analyzed and quantified.[49] As a result, 2353 proteins were detected in the control and treatment samples, with 2107 proteins (89.5%) holding quantitative information (MS-identified information and Table S1). At the filtering conditions of fold changes >1.5, $p<0.05$,

303 314 proteins were differentially expressed in response to $\mathbf{C_{10}}$ stimulation. Among the
304 314 proteins, 161 and 153 proteins were upregulated and downregulated, respectively
305 (Figures 11a and 11b). GO categories divided into BP, CC, and MF were used to
306 clarify the biological functions.[50-52] As shown in Figure 12, the BP analysis suggested
307 that proteins differently expressed were associated with single-organism process,
308 metabolic process, cellular process, localization, biological regulation, signaling,
309 response to stimulus, cellular component organization or biogenesis, and locomotion.
310 The proteins involved in the single-organism process, cellular process, and metabolic
311 process were significantly enriched (Figure 12a). In the CC category (Figure 12b),
312 proteins experiencing great changes were located in the macromolecular complex,
313 cell, membrane, organelle, extracellular region, virion, and nucleoid. In the MF
314 analysis (Figure 12c), varying levels of proteins involved in molecular transducer
315 activity, catalytic activity, binding, structural molecular activity, and antioxidant
316 activity were dramatically expressed. In addition, these changed proteins mainly
317 located in the cytoplasm from the subcellular structure location pattern (Figure S3).
318 This result showed that $\mathbf{C_{10}}$ could regulate and disturb many aspects of physiological
319 processes and functions of pathogen *Xoo*.

320 To elucidate the bacterial pathways affected by compound $\mathbf{C_{10}}$, we performed a
321 KEGG analysis. The result showed that "ribosome," "biotin metabolism,"
322 "cyanoamino acid metabolism," "other glycan degradation," and "RNA polymerase
323 biogenesis" were the distinct pathways enriched. In particular, "ribosome," which
324 plays a significant role in protein translation, was the most prominent pathway

325 involving a considerable amount of these differentially expressed proteins (Figure
326 S4).[53-55] As illustrated in Figure S5, a variety of prominent proteins were
327 downregulated, and they included the large subunit ribosomal protein L1 (rp1A),
328 protein L4 (rp1D), protein L5 (rp1E), protein L6 (rp1F), protein L10 (rp1J), protein
329 L11 (rp1K), protein L17 (rp1Q), and protein L27 (rpmA); as well as the small subunit
330 ribosomal protein S1 (rpsA), protein S5 (rpsE), and protein S13 (rpsM). These
331 proteins were significant components of the ribosome participating in various actions
332 in the protein translation program. However, their distinct downregulated expression
333 triggered by compound $\mathbf{C_{10}}$ would significantly disrupt the pathways of ribosome
334 assembly and the subsequent synthesis of a mass of functional proteins that are
335 essential for normal life, finally leading to bacterial death. To further understand the
336 significance and extent of these differentially expressed proteins in the ribosome
337 pathway, we generated a protein–protein interaction network using STRING database
338 version 10.5. As shown in Figure S6, the formed interaction relationship containing
339 11 down-regulated proteins indicated that these proteins serving as significant factors
340 could affect one another and consequently regulate and disorganize various
341 physiological processes triggered by $\mathbf{C_{10}}$ stimulation.

342 To study the morphological changes before and after treatment of *Xoo* with
343 compound $\mathbf{C_{10}}$, we obtained SEM images via a concentration-dependent manner. The
344 *Xoo* morphology was switched from well-shaped (Figure 13a) to partially broken or
345 distorted after treatment of *Xoo* with $\mathbf{C_{10}}$ (10 μg/mL) (Figure 13b). Further elevating
346 the drug dose to 25 μg/mL resulted in completely broken bacteria with large leakage

347 holes (Figure 13c). This outcome indicated that thiazolium-labeled 1,3,4-oxadiazole
348 thioethers possessed the special ability to damage the cell membrane by the
349 synergistic effects of hydrophilic and hydrophobic parts. To examine the changes of
350 membrane permeability, we used a typical dye propidium iodide (PI) without
351 fluorescence. This dye can provide significant red fluorescence after binding with
352 DNA, but it cannot thread the intact membrane of a living pathogen.[10,56] As shown in
353 Figure 13d, an enhanced fluorescent intensity at 598 nm was observed with increasing
354 drug dosages of $\mathbf{C_{10}}$, thereby demonstrating that bacterial membrane permeability
355 gradually increased and formed a PI-DNA complex to create fluorescence. This
356 outcome was in accordance with the observed SEM images. The results of
357 quantitative proteomics, SEM images, and fluorescence spectrum confirmed that title
358 molecules significantly affected the diverse physiological processes of pathogens and
359 consequently resulted in bacterial death.

360 The antifungal ability of the target molecules against an array of fungal strains,
361 namely, *G. zeae*, *F. oxysporum*, and *P. cinnamomic*, was examined via the poison
362 plate technique.[57,58] Meanwhile, the agricultural antifungal agents vitavax (**VT**),
363 prochloraz (**PC**), hymexazol (**HM**), and carbendazim (**CB**) were used as the reference
364 drugs. The preliminary screening results (Table 6) revealed that most target
365 compounds exhibited superior potency against three fungal strains relative to **VT**.
366 Moreover, some of them exhibited better toxic effects than **HM** at 50 μg/mL. All title
367 molecules exhibited moderate activity against *G. zeae* with the inhibition rates within
368 38.8%-57.9%, which were lower than that for **HM** (61.8%). A scene for inhibition

369 rates against *F. oxysporum* indicated that most of the title compounds performed
370 admirable growth suppression effects in comparison with **HM** (56.4%) and **VT**
371 (15.7%). Specifically, compounds $\mathbf{A_8}$, $\mathbf{A_{12}}$, $\mathbf{B_8}$, $\mathbf{B_{12}}$, and $\mathbf{D_{10}}$ afforded excellent
372 inhibition values of 80.5%, 73.1%, 72.1%, 77.8%, and 71.2%, respectively. For
373 anti-*P. cinnamomi* activity, compounds $\mathbf{A_8}$, $\mathbf{A_{10}}$, $\mathbf{B_8}$, $\mathbf{B_{10}}$, $\mathbf{B_{12}}$, $\mathbf{C_3}$, $\mathbf{C_7}$, $\mathbf{C_8}$, $\mathbf{C_{10}}$, $\mathbf{D_6}$, $\mathbf{D_7}$,
374 and $\mathbf{D_{10}}$ exerted powerful antibiotic performance in comparison with **HM** (50.5%),
375 with the inhibition rates exceeding 61.1%; $\mathbf{D_{10}}$, in particular, afforded the highest rate
376 of 71.6%. These investigations indicated that these compounds could be considered as
377 novel compounds in the exploration of antifungal drugs.

378 In summary, a class of thiazolium-labeled 1,3,4-oxadiazole thioethers was
379 constructed. Antibacterial results showed that compounds $\mathbf{C_{10}}$, $\mathbf{D_1}$, and $\mathbf{D_7}$ could
380 severely attack three tested phytopathogens, including *Xoo*, *R. solanacearum* and *Xac*,
381 with EC_{50} of 0.10, 3.27, and 3.50 μg/mL, respectively. Subsequently, 3D-QSAR
382 models against *Xoo* were established to direct the following excogitation for
383 discovering higher active drugs. In vivo study showed that $\mathbf{C_{10}}$ presented excellent
384 curative and protective activities (48.5% and 51.5%, 200 μg/mL) against bacterial
385 blight. Quantitative proteomic profiles indicated that 314 proteins (161 and 153
386 proteins were upregulated and downregulated, respectively) were observed to be
387 differentially expressed in response to $\mathbf{C_{10}}$ stimulation, suggesting that this kind of
388 compounds could regulate and disturb many aspects of physiological processes and
389 functions of pathogens. Scanning electron microscopy images and fluorescence
390 spectrum further confirmed this outcome. Moreover, some target compounds

391 performed superior inhibitory actions against three tested fungal strains. Given their
392 simple molecular architecture and highly efficient bioactivity, these substrates could
393 be further developed as promising surrogates for fighting against microbial infections.

394 **Supporting Information**

395 Supporting Information including detailed experimental section, Tabel S1, Figures
396 S1-S6, experimental characterization data of title compounds, ^{1}H NMR, ^{13}C NMR,
397 ^{19}F NMR, HRMS spectra and HPLC analysis associated with this article can be
398 found, in the online version.

399 **Funding Sources**

400 We thank funds from China's NNSF (21877021, 21702037, 31860516, 21662009),
401 R.P. Ministry of Education (20135201110005, 213033A), and Guizhou PS&TP (LH
402 [2017]7259, [2012]6012, [2017]5788).

403 **Conflict of interest**

404 The authors declare no competing financial interest.

405 **References**

406 (1) Morel, C.; Stermitz, F. R.; Tegos, G.; Lewis, K. Isoflavones as potentiators of
407 antibacterial activity. *J. Agric. Food Chem.* **2003**, *51*, 5677-5679.

408 (2) Wang, P. Y.; Chen, L.; Zhou, J.; Fang, H. S.; Wu, Z. B.; Song, B. A.; Yang,
409 S. Synthesis and bioactivities of 1-aryl-4-hydroxy-1*H*-pyrrol-2(5*H*)-one derivatives
410 bearing 1,3,4-oxadiazole moiety. *J. Saudi Chem. Soc.* **2017**, *21*, 315-323.

411 (3) Levy, S. B.; Marshall, B. Antibacterial resistance worldwide: causes,
412 challenges and responses. *Nat. Med*. **2004**, *10*, S122-S129.

413 (4) Hsieh, P. C.; Siegel, S. A.; Rogers, B.; Davis, D.; Lewis, K. Bacteria lacking
414 a multidrug pump: A sensitive tool for drug discovery. *Proc. Nat. Acad. Sci. USA*
415 **1998**, *95*, 6602-6606.
416 (5) Li, P.; Hu, D. Y.; Xie, D. D.; Chen, J. X.; Jin, L. H.; Song, B. A. Design,
417 synthesis, and evaluation of new sulfone derivatives containing a 1,3,4-oxadiazole
418 moiety as active antibacterial agents. *J. Agric. Food Chem*. **2018**, *66*, 3093-3100.
419 (6) Tejero, R.; Gutierrez, B.; Lopez, D.; Lopez-Fabal, F.; Gomez-Garces, J. L.;
420 Fernandez-Garcia, M. Copolymers of acrylonitrile with quaternizable thiazole and
421 triazole side-chain methacrylates as potent antimicrobial and hemocompatible
422 systems. *Acta Biomater.* **2015**, *25*, 86-96.
423 (7) Davies, J.; Davies, D. Origins and evolution of antibiotic resistance.
424 *Microbiol. Mol. Biol. Rev*. **2010**, *74*, 417-433.
425 (8) Dai, X. M.; Zhao, Y.; Li, J. S.; Li, S.; Lei, R. D.; Chen, X. L.; Zhang, X. E.;
426 Li, C. X. Thiazolium-derivative functionalized silver nanocomposites for suppressing
427 bacterial resistance and eradicating biofilms. *New J. Chem.* **2018**, *42*, 1316-1325.
428 (9) Li, P.; Tian, P. Y.; Chen, Y. Z.; Song, X. P.; Xue, W.; Jin, L. H.; Hu, D. Y.;
429 Yang, S.; Song, B. A. Novel bisthioether derivatives containing a 1,3,4-oxadiazole
430 moiety: design, synthesis, antibacterial and nematocidal activities. *Pest Manag. Sci*.
431 **2018**, *74*, 844-852.
432 (10) Zhou, J.; Tao, Q. Q.; Wang, P. Y.; Shao, W. B.; Wu, Z. B.; Li, Z.; Yang, S.
433 Antimicrobial evaluation and action mechanism of pyridinium-decorated
434 1,4-pentadien-3-one derivatives. *Bioorg. Med. Chem. Lett*. **2018**, *28*, 1742-1746.

435 (11) He, H. F.; Wang, W.; Zhou, Y.; Xia, Q.; Ren, Y. L.; Feng, J. T.; Peng, H.; He,
436 H. W.; Feng, L. L. Rational design, synthesis and biological evaluation of
437 1,3,4-oxadiazole pyrimidine derivatives as novel pyruvate dehydrogenase complex E1
438 inhibitors. *Bioorg. Med. Chem.* **2016**, *24*, 1879-1888.

439 (12) Kim, M. K.; Choi, G. J.; Lee, H. S. Fungicidal property of Curcuma longa L.
440 rhizome-derived curcumin against phytopathogenic fungi in a greenhouse. *J. Agric.*
441 *Food Chem.* **2003**, *51*, 1578-1581.

442 (13) Widsten, P.; Cruz, C. D.; Fletcher, G. C.; Pajak, M. A.; McGhie, T. K.
443 Tannins and Extracts of Fruit Byproducts: Antibacterial Activity against Foodborne
444 Bacteria and Antioxidant Capacity. *J. Agric. Food Chem.* **2014**, *62*, 11146-11156.

445 (14) Rodrigues, T.; Reker, D.; Schneider, P.; Schneider, G. Counting on natural
446 products for drug design. *Nat. Chem*. **2016**, *8*, 531-541.

447 (15) Li, H. N.; Sun, B. J.; Wang, M. Y.; Hu, X.; Gao, X.; Xu, S. T.; Xu, Y. N.; Xu,
448 J. Y.; Hua, H. M.; Li, D. H. Bioactive enmein-type 6,7-seco-ent-kaurane diterpenoids:
449 natural products, synthetic derivatives and apoptosis related mechanism. *Arch.*
450 *Pharm. Res.* **2018**, *41*, 1051-1061.

451 (16) Newman, D. J.; Cragg, G. M. Natural products as sources of new drugs from
452 1981 to 2014. *J. Nat. Prod*. **2016**, *79*, 629-661.

453 (17) Bauer, A.; Bronstrupt, M. Industrial natural product chemistry for drug
454 discovery and development. *Nat. Prod. Rep*. **2014**, *31*, 35-60.

455 (18) Zhou, Y.; Zhang, S. S.; He, H. W.; Jiang, W.; Hou, L. F.; Xie, D.; Cai, M.;
456 Peng, H.; Feng, L. L. Design and synthesis of highly selective pyruvate

457 dehydrogenase complex E1 inhibitors as bactericides. *Bioorg. Med. Chem*. **2018**, *26*,
458 84-95.
459 (19) Arjunan, P.; Sax, M.; Brunskill, A.; Chandrasekhar, K.; Nemeria, N.; Zhang,
460 S.; Jordan, F.; Furey, W. A thiamin-bound, pre-decarboxylation reaction intermediate
461 analogue in the pyruvate dehydrogenase E1 subunit induces large scale
462 disorder-to-order transformations in the enzyme and reveals novel structural features
463 in the covalently bound adduct. *J. Biol. Chem*. **2006**, *281*, 15296-15303.
464 (20) Klaus, A.; Pfirrmann, T.; Glomb, M. A. Transketolase A from E-coli
465 Significantly Suppresses Protein Glycation by Glycolaldehyde and Glyoxal in Vitro.
466 *J. Agric. Food Chem*. **2017**, *65*, 8196-8202.
467 (21) Snyder, H. R. J.; Benjamin, L. E. Nitrofuryl heterocytes. IX. Some
468 derivatives and analogs of
469 6,7-dihydro-3-(5-nitro-2-furyl)-5H-imidazo[2,1-b]thiazolium chloride. *J. Med. Chem.*
470 **1970**, *13*, 164-165.
471 (22) Kim, S. H.; Son, H.; Nam, G.; Chi, D. Y.; Kim, J. H. Synthesis and in vitro
472 antibacterial activity of 3-[N-methyl-N-(3-methyl-1,3-thiazolium-2-yl)aminolmethyl
473 cephalosporin derivatives. *Bioorg. Med. Chem. Lett*. **2000**, *10*, 1143-1145.
474 (23) Ben Mamoun, C.; Prigge, S. T.; Vial, H. Targeting the Lipid Metabolic
475 Pathways for the Treatment of Malaria. *Drug Dev. Res.* **2010**, *71*, 44-55.
476 (24) Hamze, A.; Rubi, E.; Arnal, P.; Boisbrun, M.; Carcel, C.; Salom-Roig, X.;
477 Maynadier, M.; Wein, S.; Vial, H.; Calas, M. Mono- and bis-thiazolium salts have
478 potent antimalarial activity. *J. Med. Chem*. **2005**, *48*, 3639-3643.

479 (25) Nicolas, O.; Margout, D.; Taudon, N.; Wein, S.; Calas, M.; Vial, H. J.;
480 Bressolle, F. M. M. Pharmacological properties of a new antimalarial bisthiazolium
481 salt, T3, and a corresponding prodrug, TE3. *Antimicrob. Agents Ch*. **2005**, *49*,
482 3631-3639.

483 (26) Cui, Z. N.; Shi, Y. X.; Zhang, L.; Ling, Y.; Li, B. J.; Nishida, Y.; Yang, X. L.
484 Synthesis and fungicidal activity of novel 2,5-disubstituted-1,3,4-oxadiazole
485 derivatives. *J. Agric. Food Chem*. **2012**, *60*, 11649-11656.

486 (27) Behalo, M. S. An efficient one-pot catalyzed synthesis of
487 2,5-disubstituted-1,3,4-oxadiazoles and evaluation of their antimicrobial activities.
488 *RSC Adv*. **2016**, *6*, 103132-103136.

489 (28) Wet-osot, S.; Phakhodee, W.; Pattarawarapan, M. Application of
490 N-acylbenzotriazoles in the synthesis of 5-substituted 2-ethoxy-1,3,4-oxadiazoles as
491 building blocks toward 3,5-disubstituted 1,3,4-oxadiazol-2(3H)-ones. *J. Org. Chem*.
492 **2017**, *82*, 9923-9929.

493 (29) Tao, Q. Q.; Liu, L. W.; Wang, P. Y.; Long, Q. S.; Zhao, Y. L.; Jin, L. H.; Xu,
494 W. M.; Chen, Y.; Li, Z.; Yang, S. Synthesis and In Vitro and In Vivo Biological
495 Activity Evaluation and Quantitative Proteome Profiling of Oxadiazoles Bearing
496 Flexible Heterocyclic Patterns. *J. Agric. Food Chem.* **2019**, *67*, 7626-7639.

497 (30) Du, Q. R.; Li, D. D.; Pi, Y. Z.; Li, J. R.; Sun, J.; Fang, F.; Zhong, W. Q.;
498 Gong, H. B.; Zhu, H. L. Novel 1,3,4-oxadiazole thioether derivatives targeting
499 thymidylate synthase as dual anticancer/antimicrobial agents. *Bioorg. Med. Chem*.
500 **2013**, *21*, 2286-2297.

501 (31) Desai, N. C.; Kotadiya, G. M.; Trivedi, A. R.; Khedkar, V. M.; Jha, P. C.
502 Design, synthesis, and biological evaluation of novel fluorinated pyrazole
503 encompassing pyridyl 1,3,4-oxadiazole motifs. *Med. Chem. Res.* **2016**, *25*,
504 2698-2717.

505 (32) Manjunatha, K.; Poojary, B.; Lobo, P. L.; Fernandes, J.; Kumari, N. S.
506 Synthesis and biological evaluation of some 1,3,4-oxadiazole derivatives. *Eur. J.*
507 *Med. Chem*. **2010**, *45*, 5225-5233.

508 (33) Xu, W. M.; Han, F. F.; He, M.; Hu, D. Y.; He, J.; Yang, S.; Song, B. A.
509 Inhibition of tobacco bacterial wilt with sulfone derivatives containing an
510 1,3,4-oxadiazole moiety. *J. Agric. Food Chem*. **2012**, *60*, 1036-1041.

511 (34) Fizazi, K. S.; Higano, C. S.; Nelson, J. B.; Gleave, M.; Miller, K.; Morris, T.;
512 Nathan, F. E.; McIntosh, S.; Pemberton, K.; Moul, J. W. Phase III, randomized,
513 placebo-controlled study of docetaxel in combination with zibotentan in patients with
514 metastatic castration-resistant prostate cancer. *J. Clin. Oncol.* **2013**, *31*, 1740-1748.

515 (35) Khan, P. R.; Durgaprasad, M.; Reddy, S. G.; Reddy, G. R.; Hussein, I. A.;
516 Reddy, B. V. S. IBX/KI promoted synthesis of 2,5-disubstituted 1,3,4-oxadiazoles.
517 *Lett. Org. Chem.* **2018**, *15*, 64-69.

518 (36) McMahon, D.; Jones, J.; Wiegand, A.; Gange, S. J.; Kearney, M.; Palmer, S.;
519 McNulty, S.; Metcalf, J. A.; Acosta, E.; Rehm, C.; Coffin, J. M.; Mellors, J. W.;
520 Maldarelli, F. Short-course raltegravir intensification does not reduce persistent
521 low-level viremia in patients with HIV-1 suppression during receipt of combination
522 antiretroviral therapy. *Clin. Infect. Dis.* **2010**, *50*, 912-919.

523 (37) Sarshira, E. M.; Hamada, N. M.; Moghazi, Y. M.; Abdelrahman, M. M.
524 Synthesis and biological evaluation of some heterocyclic compounds from salicylic
525 acid hydrazide[1]. *J. Heterocylic Chem.* **2016**, *53*, 1970-1982.
526 (38) Li, P.; Yin, J.; Xu, W. M.; Wu, J.; He, M.; Hu, D. Y.; Yang, S.; Song, B. A.
527 Synthesis, Antibacterial Activities, and 3D-QSAR of Sulfone Derivatives Containing
528 1,3,4-Oxadiazole Moiety. *Chem. Biol. Drug Des.* **2013**, *82*, 546–556.
529 (39) Arnoldi, A.; Carzaniga, R.; Morini, G.; Merlini, L.; Farina, G. Synthesis,
530 fungicidal activity, and QSAR of a series of 2-dichlorophenyl-3-triazolylpropyl
531 ethers. *J. Agric. Food Chem*. **2000**, *48*, 2547-2555.
532 (40) Friggeri, L.; Hargrove, T. Y.; Wawrzak, Z.; Blobaum, A. L.; Rachakonda,
533 G.; Lindsley, C. W.; Villalta, F.; Nes, W. D.; Botta, M.; Guengerich, F. P.;
534 Lepesheva, G. I. Sterol 14 alpha-Demethylase Structure-Based Design of VNI
535 ((R)-N-(1-(2,4-Dichlorophenyl)-2-(1H-imidazol-1-yl)ethyl)-4-(5-phenyl-1,3,4-oxadia
536 zol-2-yl)benzamide)) Derivatives To Target Fungal Infections: Synthesis, Biological
537 Evaluation, and Crystallographic Analysis. *J. Med. Chem*. **2018**, *61*, 5679-5691.
538 (41) Arnoldi, A.; Dallavalle, S.; Merlini, L.; Musso, L.; Farina, G.; Moretti, M.;
539 Jayasinghe, L. Synthesis and antifungal activity of a series of N-substituted
540 [2-(2,4-dichlorophenyl)-3-(1,2,4-triazol-1-yl)]propylamines. *J. Agric. Food Chem*.
541 **2007**, *55*, 8187-8192.
542 (42) Amjadi, M.; Jalili, R. Molecularly imprinted mesoporous silica embedded
543 with carbon dots and semiconductor quantum dots as a ratiometric fluorescent sensor
544 for diniconazole. *Biosens. Bioelectron*. **2017**, *96*, 121-126.

545 (43) Mustafa, I. F.; Hussein, M. Z.; Saifullah, B.; Idris, A.; Hilmi, N. H. Z.;
546 Fakurazi, S. Synthesis of (Hexaconazole-Zinc/Aluminum-Layered Double Hydroxide
547 Nanocomposite) Fungicide Nanodelivery System for Controlling Ganoderma Disease
548 in Oil Palm. *J. Agric. Food Chem.* **2018**, *66*, 806-813.

549 (44) Wang, P. Y.; Fang, H. S.; Shao, W. B.; Zhou, J.; Chen, Z.; Song, B. A.;
550 Yang, S. Synthesis and biological evaluation of pyridinium-functionalized carbazole
551 derivatives as promising antibacterial agents. *Bioorg. Med. Chem. Lett.* **2017**, *27*,
552 4294-4297.

553 (45) Wang, P. Y.; Zhou, L.; Zhou, J.; Wu, Z. B.; Xue, W.; Song, B. A.; Yang, S.
554 Synthesis and antibacterial activity of pyridinium-tailored
555 2,5-substituted-1,3,4-oxadiazole thioether/sulfoxide/sulfone derivatives. *Bioorg. Med.*
556 *Chem. Lett.* **2016**, *26*, 1214-1217.

557 (46) Fang, C.; Kong, L. L.; Ge, Q.; Zhang, W.; Zhou, X. J.; Zhang, L.; Wang, X.
558 P. Antibacterial activities of N-alkyl imidazolium-based poly(ionic liquid)
559 nanoparticles. *Polym. Chem*. **2019**, *10*, 209-218.

560 (47) Chien, H. W.; Chen, Y. Y.; Chen, Y. L.; Cheng, C. H.; Lin, J. C.; Studies of
561 PET nonwovens modified by novel antimicrobials configured with both N-halamine
562 and dual quaternary ammonium with different alkyl chain length. *RSC Adv.* **2019**, *9*,
563 7257-7265.

564 (48) Song, X. P.; Li, P.; Li, M. W.; Yang, A. M.; Yu, L.; Luo, L. Z.; Hu, D. Y.;
565 Song, B. A. Synthesis and investigation of the antibacterial activity and action
566 mechanism of 1,3,4-oxadiazole thioether derivatives. *Pestic. Biochem. Phys*. **2018**,

567 *147*, 11-19.

568 (49) Wang, Y. M.; Gupta, R.; Song, W.; Huh, H. H.; Lee, S. E.; Wu, J. N.;
569 Agrawal, G. K.; Rakwal, R.; Kang, K. Y.; Park, S. R.; Kim, S. T. Label-free
570 quantitative secretome analysis of Xanthomonas oryzae pv. oryzae highlights the
571 involvement of a novel cysteine protease in its pathogenicity. *J. Proteomics* **2017**,
572 *169*, 202-214.

573 (50) Chen, J.; Shi, J.; Yu, L.; Liu, D. Y.; Gan, X. H.; Song, B. A.; Hu, D. Y.
574 Design, Synthesis, Antiviral Bioactivity, and Defense Mechanisms of Novel
575 Dithioacetal Derivatives Bearing a Strobilurin Moiety. *J. Agric. Food Chem.* **2018**,
576 *66*, 5335-5345.

577 (51) Chen, X. L.; Xie, X.; Wu, L. Y.; Liu, C. Y.; Zeng, L. R.; Zhou, X. P.; Luo, F.;
578 Wang, G. L.; Liu, W. D. Proteomic Analysis of Ubiquitinated Proteins in Rice (Oryza
579 sativa) After Treatment With Pathogen-Associated Molecular Pattern (PAMP)
580 Elicitors. *Front. Plant Sci.* **2018**, *9*, DOI: 10.3389/fpls.2018.01064.

581 (52) Zhao, Y. L.; Huang, X.; Liu, L. W.; Wang, P. Y.; Long, Q. S.; Tao, Q. Q.; Li,
582 Z.; Yang, S. Identification of Racemic and Chiral Carbazole Derivatives Containing
583 an Isopropanolamine Linker as Prospective Surrogates against Plant Pathogenic
584 Bacteria: In Vitro and In Vivo Assays and Quantitative Proteomics. *J. Agric. Food*
585 *Chem.* **2019**, *67*, 7512-7525.

586 (53) Wilson, D. N. Ribosome-targeting antibiotics and mechanisms of bacterial
587 resistance. *Nat. Rev. Microbiol.* **2014**, *12*, 35-48.

588 (54) Lai, W. J. C.; Ermolenko, D. N. Ensemble and single-molecule FRET studies

589 of protein synthesis. *Methods* **2018**, *137*, 37-48.

590 (55) de Loubresse, N. G.; Prokhorova, I.; Holtkamp, W.; Rodnina, M. V.;
591 Yusupova, G.; Yusupov, M. Structural basis for the inhibition of the eukaryotic
592 ribosome. *Nature* **2014**, *513*, 517-522.

593 (56) Kong, J.; Zhang, Y.; Ju, J.; Xie, Y. F.; Guo, Y. H.; Cheng, Y. L.; Qian, H.;
594 Quek, S. Y.; Yao, W. R. Antifungal effects of thymol and salicylic acid on cell
595 membrane and mitochondria of Rhizopus stolonifer and their application in
596 postharvest preservation of tomatoes. *Food Chem.* **2019**, *285*, 380-388.

597 (57) Chattapadhyay, T. K.; Dureja, P. Antifungal activity of
598 4-methyl-6-alkyl-2H-pyran-2-ones. *J. Agric. Food Chem.* **2006**, *54*, 2129-2133.

599 (58) Heise, T.; Schmidt, F.; Knebel, C.; Rieke, S.; Haider, W.; Geburek, I.;
600 Niemann, L.; Marx-Stoelting, P. Hepatotoxic combination effects of three azole
601 fungicides in a broad dose range. *Arch. Toxicol*. **2018**, *92*, 859-872.

602 **Figure captions**

603 **Figure 1.** Some bioactive structures containing thiazolium, 1,3,4-oxadiazole, or
604 2,4-dichlorophenyl scaffolds.

605 **Figure 2.** Design strategy for target molecules.

606 **Figure 3.** Synthetic route for $\mathbf{A_n}$ and $\mathbf{B_n}$ (n = 6, 8, 10, 12).

607 **Figure 4.** Synthetic route for $\mathbf{C_n}$ and $\mathbf{D_n}$ (n = 1–10).

608 **Figure 5.** Crystal structures of compound $\mathbf{D_7}$.

609 **Figure 6.** Molecular alignment of all target compounds.

610 **Figure 7.** Plots of predicted pEC_{50} versus experimental pEC_{50} against *Xoo*. Predicted
611 pEC_{50} values were calculated for A) CoMFA model and B) CoMSIA model.

612 **Figure 8.** CoMFA contour maps with compound $\mathbf{C_{10}}$ inside the fields: A) steric fields,
613 with green and yellow polyhedra indicating the regions where steric bulk would
614 enhance and reduce the activity; B) electrostatic fields, with blue and red polyhedra
615 indicating the regions where positive and negative charges would enhance activity.

616 **Figure 9.** CoMSIA contour maps with compound $\mathbf{C_{10}}$ inside the fields: A) steric
617 fields, with green and yellow polyhedra indicating the regions where steric bulk
618 would enhance and reduce the activity; B) electrostatic fields, with blue and red
619 polyhedra indicating the regions where positive and negative charges would enhance
620 activity; C) hydrophobic fields, with yellow and grey polyhedra indicating the regions
621 where hydrophobicity and hydrophilicity would enhance activity; D) H-bond acceptor
622 fields, with red contours indicating the regions where H-bond acceptor groups would
623 enhance activity.

624 **Figure 10.** Curative and protection activities of compound $\mathbf{C_{10}}$ against rice bacterial
625 leaf blight under greenhouse conditions at 200 μg/mL; **BT** and **TC** were the positive
626 control at the same conditions.

627 **Figure 11.** a) Histogram of the number distribution of differentially expressed
628 proteins in different comparison groups ($\mathbf{C_{10}}$**/CK**); b) volcano plot of differentially
629 expressed proteins ($\mathbf{C_{10}}$**/CK**).

630 **Figure 12.** Differentially expressed proteins in control and treatment groups were
631 classified on the basis of known biological processes (a), cellular components (b), and
632 molecular functions (c).

633 **Figure 13.** SEM images of *Xoo* after incubation in different concentrations of $\mathbf{C_{10}}$: (a)
634 0, (b) 10, and (c) 25 μg/mL; the scale bars for (a–c) are 1 μm; (d) fluorescence
635 intensities stained with PI for the solution containing *Xoo* after incubating with
636 different concentrations of $\mathbf{C_{10}}$.

637 **Tables**

638 **Table 1.** Antibacterial effects of $\mathbf{A_n}$ and $\mathbf{B_n}$ against *Xoo*, *R. solanacearum,* and *Xac* in

639 vitro.

Compd.	*Xoo*			*R. solanacearum*			*Xac*		
	Regression equation	r	EC_{50} (μg/mL)	Regression equation	r	EC_{50} (μg/mL)	Regression equation	r	EC_{50} (μg/mL)
$\mathbf{A_6}$	y=5.61x+1.16	0.97	4.84±0.78	y=2.33x+0.67	0.99	72.41±4.92	y=1.92x+3.55	0.96	5.67±0.75
$\mathbf{A_8}$	y=2.70x+3.70	1.00	3.04±0.35	y=1.39x+3.04	0.97	25.51±0.85	y=2.32x+3.42	0.99	4.78±0.15
$\mathbf{A_{10}}$	y=2.68x+6.29	0.99	0.33±0.03	y=0.71x+3.64	0.97	83.59±10.08	y=3.65x+1.41	1.00	9.62±0.41
$\mathbf{A_{12}}$	y=2.94x+6.82	0.98	0.24±0.03	y=0.87x+3.35	0.98	79.71±0.93	y=2.03x+2.71	0.99	13.44±4.00
$\mathbf{B_6}$	y=4.28x+2.88	0.97	3.12±0.35	y=2.09x+1.14	1.00	70.99±5.20	y=2.58x+3.08	0.97	5.56±0.50
$\mathbf{B_8}$	y=2.86x+4.22	0.96	1.87±0.21	y=1.87x+2.25	0.97	29.80±1.74	y=3.10x+3.20	0.97	3.80±0.28
$\mathbf{B_{10}}$	y=4.73x+6.25	0.99	0.54±0.02	y=3.17x-0.74	0.97	65.04±3.69	y=2.30x+2.13	0.98	17.58±2.88
$\mathbf{B_{12}}$	y=2.80x+6.75	0.98	0.23±0.09	y=0.76x+3.86	0.98	31.28±2.29	y=3.20x+1.31	0.95	14.27±1.19
BT	y=1.50x-2.05	0.98	92.6±2.1	/	/	/	/	/	/
TC	y=1.54x+1.79	0.98	121.8±3.6	y=1.03x+2.94	0.99	99.1±5.1	y=2.15x+0.94	0.98	77.0±2.0

640

641 **Table 2.** In vitro antibacterial effects of $\mathbf{C_n}$ and $\mathbf{D_n}$ against *Xoo*, *R. solanacearum*, and

642 *Xac*.

Compd.	*Xoo*			*R. solanacearum*			*Xac*		
	Regression equation	r	EC_{50} (μg/mL)	Regression equation	r	EC_{50} (μg/mL)	Regression equation	r	EC_{50} (μg/mL)
$\mathbf{C_1}$	y=3.48x+7.43	1.00	0.20±0.03	y=0.69x+4.36	1.00	8.45±0.64	y=3.32x+0.90	0.98	17.21±3.04
$\mathbf{C_2}$	y=3.58x+6.20	1.00	0.46±0.04	y=0.79x+3.95	0.99	21.72±1.97	y=2.48x+3.40	0.98	4.42±0.43
$\mathbf{C_3}$	y=3.15x+5.35	0.95	0.77±0.03	y=0.59x+3.88	1.00	77.93±0.16	y=2.81x+2.98	0.99	5.21±0.04
$\mathbf{C_4}$	y=3.14x+6.74	0.97	0.28±0.01	y=0.88x+3.89	0.97	18.16±2.54	y=5.02x+1.30	0.97	5.46±1.58
$\mathbf{C_5}$	y=5.22x+7.16	0.98	0.39±0.09	y=1.34x+2.86	0.95	39.94±2.76	y=2.51x+3.01	0.99	6.19±1.16
$\mathbf{C_6}$	y=4.96x+7.02	1.00	0.39±0.03	y=0.96x+3.14	1.00	85.27±0.82	y=4.32x+0.11	0.96	13.53±2.43
$\mathbf{C_7}$	y=5.39x+6.89	0.98	0.44±0.01	y=0.83x+3.54	0.95	57.23±6.25	y=2.50x+3.11	0.96	5.71±0.26
$\mathbf{C_8}$	y=2.37x+6.93	1.00	0.15±0.01	y=0.93x+3.54	0.97	36.55±0.32	y=2.86x+2.58	0.98	7.05±0.50
$\mathbf{C_9}$	y=2.99x+7.50	0.97	0.15±0.02	y=1.24x+3.02	0.98	39.26±1.54	y=3.74x+0.75	0.95	13.66±0.08
$\mathbf{C_{10}}$	y=3.78x+8.84	0.99	0.10±0.01	y=0.94x+4.08	0.99	9.59±1.04	y=3.73x+0.65	1.00	14.59±0.90
$\mathbf{D_1}$	y=3.11x+6.91	0.99	0.24±0.01	y=0.89x+4.54	0.96	3.27±0.25	y=2.63x+2.02	0.97	13.56±0.79
$\mathbf{D_2}$	y=8.15x+7.50	0.99	0.49±0.01	y=1.24x+3.69	0.98	11.37±1.48	y=5.18x+0.16	0.98	8.59±0.24
$\mathbf{D_3}$	y=3.11x+6.03	0.95	0.47±0.03	y=0.67x+3.78	1.00	66.25±4.23	y=3.47x+2.55	1.00	5.08±0.42
$\mathbf{D_4}$	y=6.89x+6.59	0.98	0.59±0.01	y=1.21x+3.64	1.00	13.42±1.29	y=3.18x+0.79	0.97	4.93±0.90
$\mathbf{D_5}$	y=5.26x+7.56	0.96	0.33±0.04	y=0.78x+3.71	0.99	43.89±7.07	y=2.39x+3.55	0.98	4.06±0.27
$\mathbf{D_6}$	y=3.55x+6.65	0.97	0.34±0.01	y=0.95x+4.16	0.97	7.59±0.52	y=4.44x+1.82	0.95	5.20±0.44
$\mathbf{D_7}$	y=1.48x+4.67	0.97	1.68±0.33	y=1.12x+3.59	0.97	18.12±2.53	y=3.18x+3.27	0.97	3.50±0.31
$\mathbf{D_8}$	y=2.31x+7.04	0.99	0.13±0.01	y=1.03x+4.28	0.98	6.66±0.57	y=0.60x+0.65	0.96	16.17±1.90
$\mathbf{D_9}$	y=1.68x+5.59	0.95	0.45±0.02	y=1.16x+4.00	0.99	7.39±0.12	y=4.19x+0.13	0.95	14.53±2.00
$\mathbf{D_{10}}$	y=5.20x+8.03	0.99	0.26±0.05	y=1.10x+4.12	1.00	6.38±0.87	y=4.14x+0.95	0.97	9.49±0.84
BT	y=1.50x-2.05	0.98	92.6±2.1	/	/	/	/	/	/
TC	y=1.54x+1.79	0.98	121.8±3.6	y=1.03x+2.94	0.99	99.1±5.1	y=2.15x+0.94	0.98	77.0±2.0

643

644 **Table 3.** Experimental and predicted pEC_{50} of title molecules against *Xoo*, * training

645 set molecules.

Compd.	Experimental pEC_{50}	CoMFA		CoMSIA	
		Predicted	Relative error	Predicted	Relative error
A_6*	5.010	5.039	-0.029	5.037	-0.027
A_8*	5.236	5.196	0.040	5.214	0.022
A_{10}*	6.223	6.281	-0.058	6.226	-0.003
A_{12}	6.383	6.446	-0.063	6.763	-0.380
B_6*	5.213	5.187	0.026	5.190	0.023
B_8*	5.458	5.474	-0.016	5.476	-0.018
B_{10}	6.020	6.119	-0.099	6.374	-0.354
B_{12}*	6.412	6.352	0.060	6.485	-0.073
C_1*	6.435	6.437	-0.002	6.428	0.007
C_2*	6.074	6.066	0.008	6.176	-0.102
C_3*	5.861	5.836	0.025	5.875	-0.014
C_4	6.276	6.034	0.242	6.240	0.036
C_5*	6.171	6.238	-0.067	6.185	-0.014
C_6*	6.154	6.129	0.025	6.157	-0.003
C_7*	6.065	5.946	0.119	5.954	0.111
C_8*	6.557	6.594	-0.037	6.537	0.020
C_9	6.557	6.482	0.075	6.154	0.403
C_{10}*	6.734	6.630	0.104	6.707	0.027
D_1*	6.367	6.263	0.104	6.288	0.079
D_2*	6.057	5.931	0.126	5.886	0.171
D_3*	6.086	6.134	-0.048	6.075	0.011
D_4*	5.964	5.870	0.094	5.927	0.037
D_5	6.254	6.090	0.164	5.883	0.371
D_6	6.224	6.032	0.192	5.886	0.338
D_7*	5.495	5.828	-0.333	5.673	-0.178
D_8	6.630	6.448	0.182	6.238	0.392
D_9	6.091	6.322	-0.231	5.849	0.242
D_{10}*	6.331	6.470	-0.139	6.407	-0.076

646

647 **Table 4.** The obtained statistical parameters of CoMFA and CoMSIA models for *Xoo*.

Statistical parameter	CoMFA	CoMSIA	Validation criterion
q^2 [a]	0.766	0.792	>0.5
ONC[b]	5	8	
r^2 [c]	0.951	0.976	>0.8
Standard error of estimate	0.123	0.098	
F-value	54.632	54.786	
Fraction of field contributions			
Steric	0.590	0.135	
Electrostatic	0.410	0.527	
Hydrophobic		0.333	
H-bond donor		0.000	
H-bond acceptor		0.005	

648 [a] Cross-validated correlation, [b] Optimum number of components, [c] Non-cross-validated correlation.

649 **Table 5.** In vivo biological activities of **C_{10}** (200 μg/mL, 14 days after spraying)

650 against rice bacterial blight.

Treatment	Curative activity			Protection activity		
	Morbidity (%)	Disease index (%)	Control efficiency (%)[b]	Morbidity (%)	Disease index (%)	Control efficiency (%)[b]
C_{10}	100	42.2	48.5	100	39.7	51.5
BT	100	55.0	32.8	100	52.4	36.1
TC	100	49.8	39.2	100	46.6	43.2
CK[a]	100	81.9	/	100	81.9	/

651 [a] Negative control. [b] Statistical analysis was conducted by ANOVA method.

652 **Table 6.** Inhibitory effects of $\mathbf{A_n}$, $\mathbf{B_n}$, $\mathbf{C_n}$, and $\mathbf{D_n}$ (dosage: 50 μg/mL) against three

653 plant fungal strains in vitro.

Compd.	Inhibition rate (%)			Compd.	Inhibition rate (%)		
	G. zeae	*F. oxysporum*	*P. cinnamomi*		*G. zeae*	*F. oxysporum*	*P. cinnamomi*
$\mathbf{A_6}$	49.1±1.1	63.5±3.1	35.7±0.6	$\mathbf{B_6}$	47.7±1.5	33.8±2.5	21.4±4.1
$\mathbf{A_8}$	50.3±2.0	80.5±3.2	69.4±2.5	$\mathbf{B_8}$	49.1±1.6	72.1±3.3	63.9±1.2
$\mathbf{A_{10}}$	50.6±0.7	67.5±0.4	65.6±1.0	$\mathbf{B_{10}}$	46.0±5.0	65.9±3.1	66.0±0.6
$\mathbf{A_{12}}$	47.7±1.3	73.1±2.5	57.8±1.7	$\mathbf{B_{12}}$	53.2±2.9	77.8±3.7	68.4±1.6
$\mathbf{C_1}$	52.6±6.6	56.9±1.2	37.8±2.5	$\mathbf{D_1}$	52.6±2.4	49.3±5.3	48.3±1.8
$\mathbf{C_2}$	50.7±2.3	51.9±1.8	47.2±2.3	$\mathbf{D_2}$	51.2±2.6	54.9±0.1	59.2±1.0
$\mathbf{C_3}$	48.7±1.3	68.5±0.4	63.3±1.2	$\mathbf{D_3}$	49.5±1.3	60.5±0.5	59.8±1.5
$\mathbf{C_4}$	51.6±0.6	52.5±1.0	45.0±2.8	$\mathbf{D_4}$	49.6±0.4	51.6±1.9	53.1±0.9
$\mathbf{C_5}$	38.8±4.7	52.2±0.9	43.4±2.1	$\mathbf{D_5}$	42.3±5.3	53.4±0.5	57.9±0.8
$\mathbf{C_6}$	56.7±2.1	64.1±6.3	59.2±1.7	$\mathbf{D_6}$	57.3±0.7	67.1±1.7	67.0±1.2
$\mathbf{C_7}$	56.5±0.3	69.2±2.0	67.6±5.0	$\mathbf{D_7}$	55.3±1.6	68.6±1.1	66.5±2.5
$\mathbf{C_8}$	57.8±5.5	63.2±2.2	61.1±1.2	$\mathbf{D_8}$	54.4±1.5	59.6±0.9	56.5±3.2
$\mathbf{C_9}$	51.8±1.7	51.9±1.8	44.8±2.9	$\mathbf{D_9}$	49.8±2.6	53.7±1.0	55.2±1.4
$\mathbf{C_{10}}$	54.1±2.1	66.5±1.6	65.1±0.9	$\mathbf{D_{10}}$	57.9±5.4	71.2±2.4	71.6±6.5
VT	44.0±2.0	15.7±0.8	20.6±1.6	**PC**	100	100	100
HM	61.8±0.8	56.4±2.4	50.5±0.9	**CB**	100	100	100

654

Figures

Figure 1

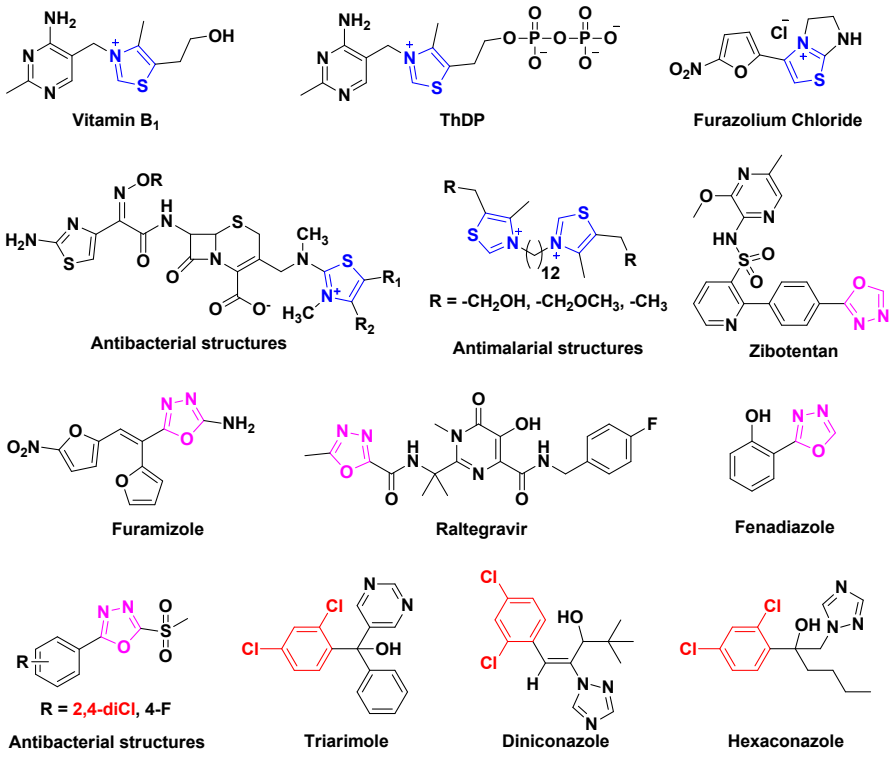

658 **Figure 2**

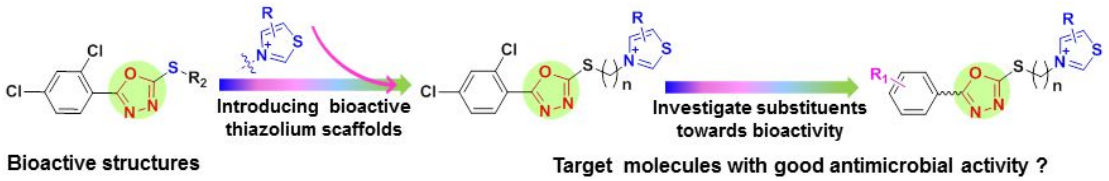

659

660 **Figure 3**

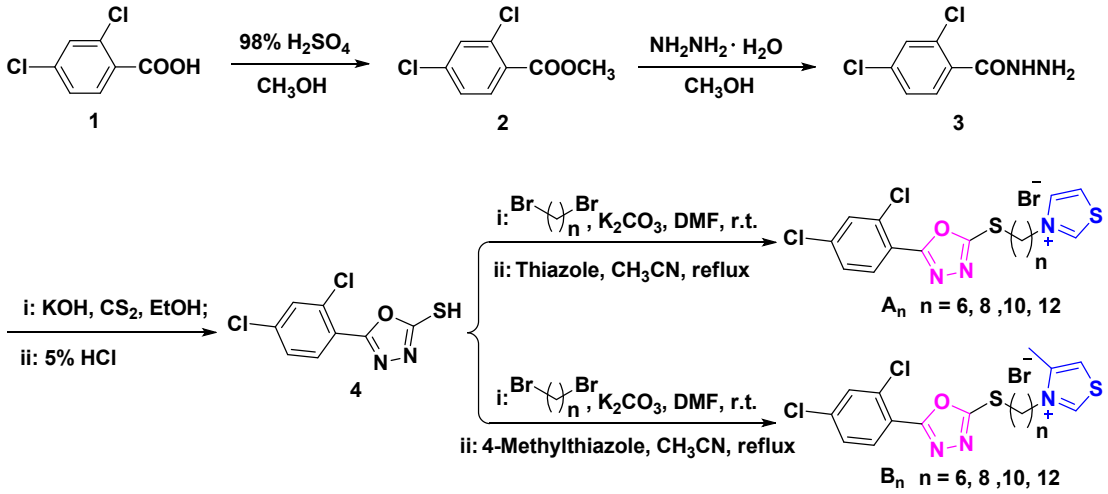

661

662 **Figure 4**

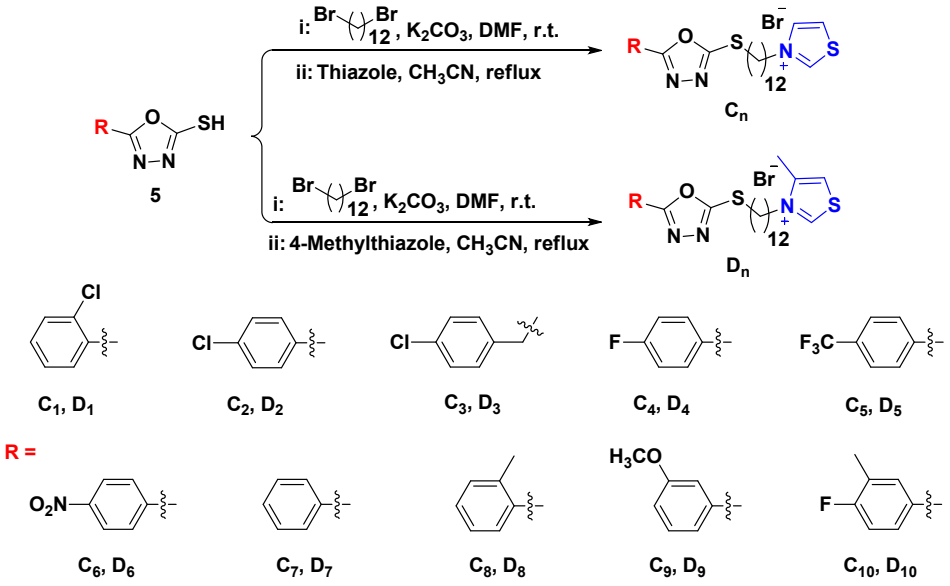

663

Figure 5

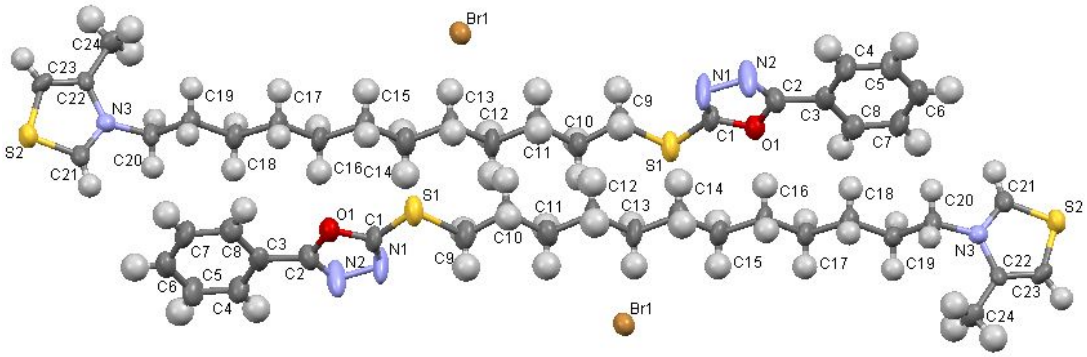
Br1
C24
C23
C22
N3
S2
C21
C20
C19
C18
C17
C16
C15
C14
C13
C12
C11
C10
C9
S1
C1
O1
N2
N1
C2
C3
C4
C5
C6
C7
C8
Br1
C21
S2
N3
C22
C23
C24
C20
C19
C18
C17
C16
C15
C14
C13
C12
C11
C10
C9
S1
C1
O1
N2
N1
C2
C3
C4
C5
C6
C7
C8

666 **Figure 6**

667 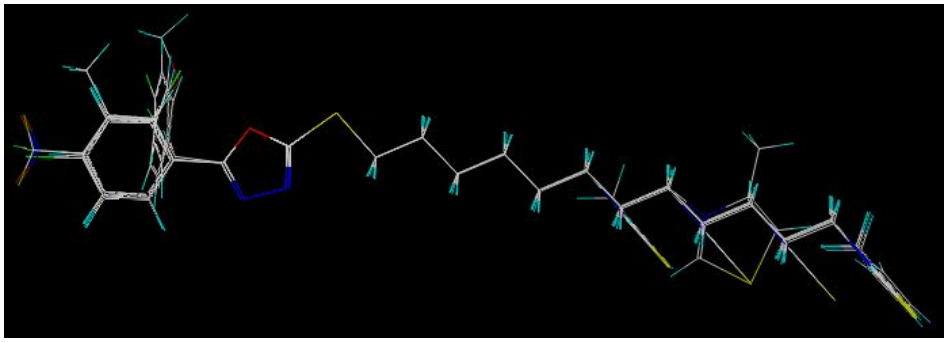

668 **Figure 7**

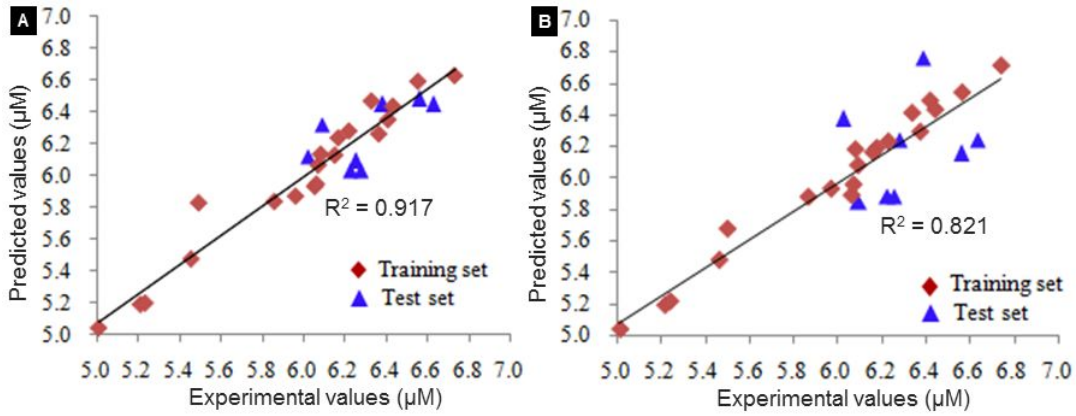

669

670 **Figure 8**

671

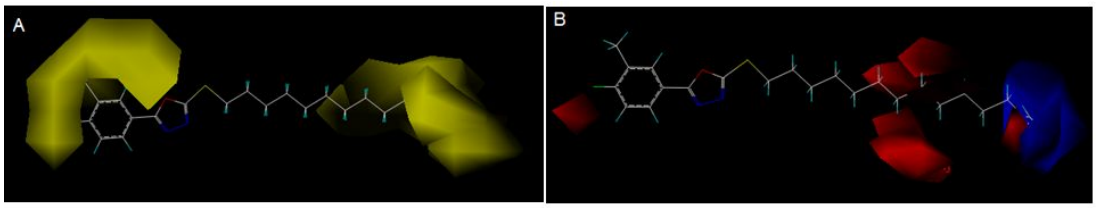

672

673 **Figure 9**

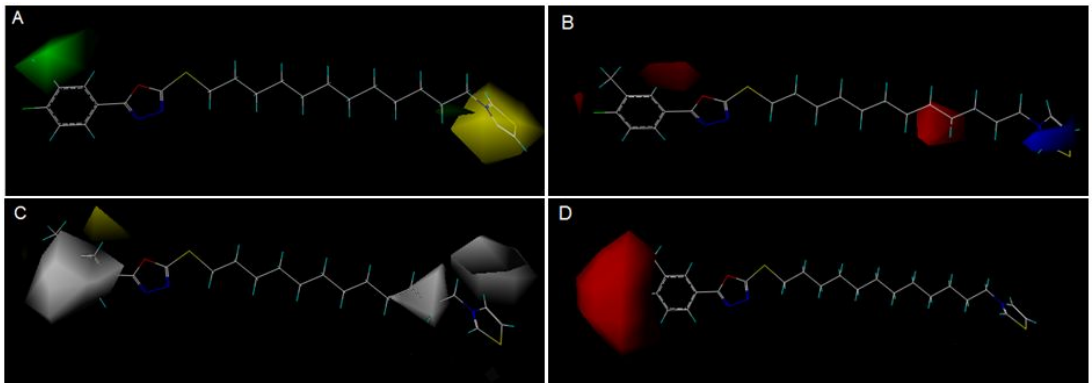

674

675 **Figure 10**

676

677 **Figure 11**

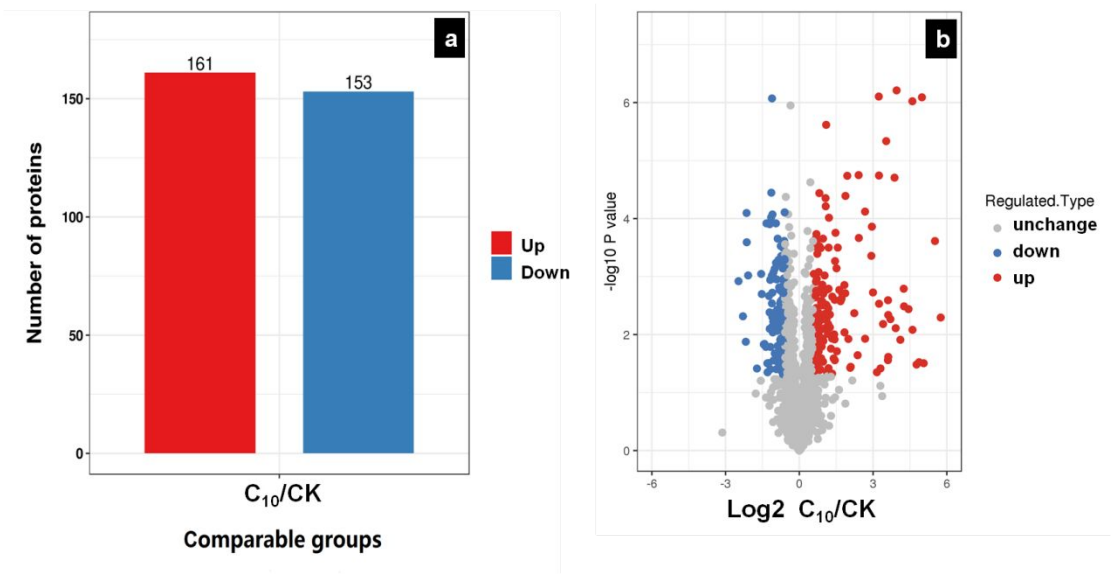

678

679

680 **Figure 12**

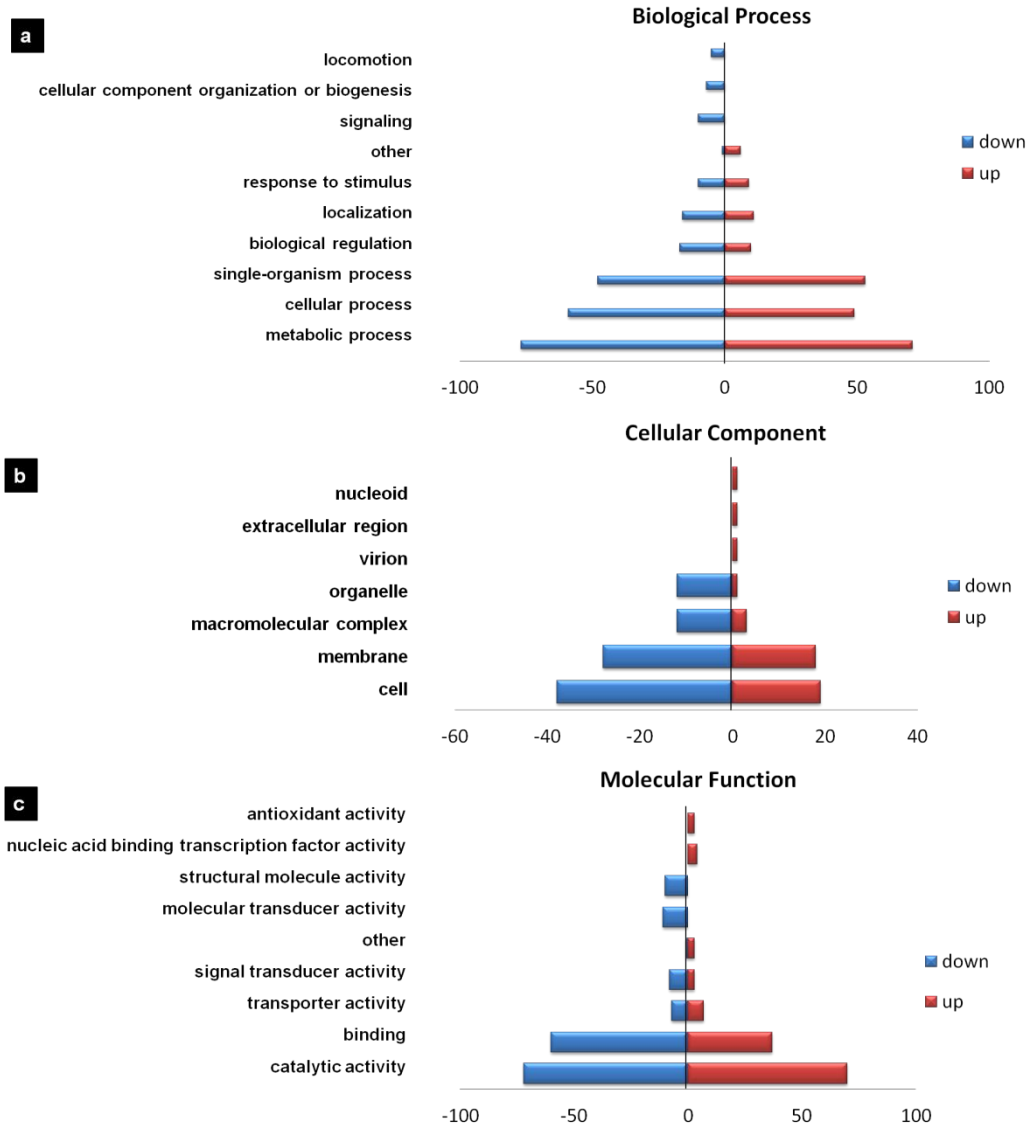

681

682

683 **Figure 13**

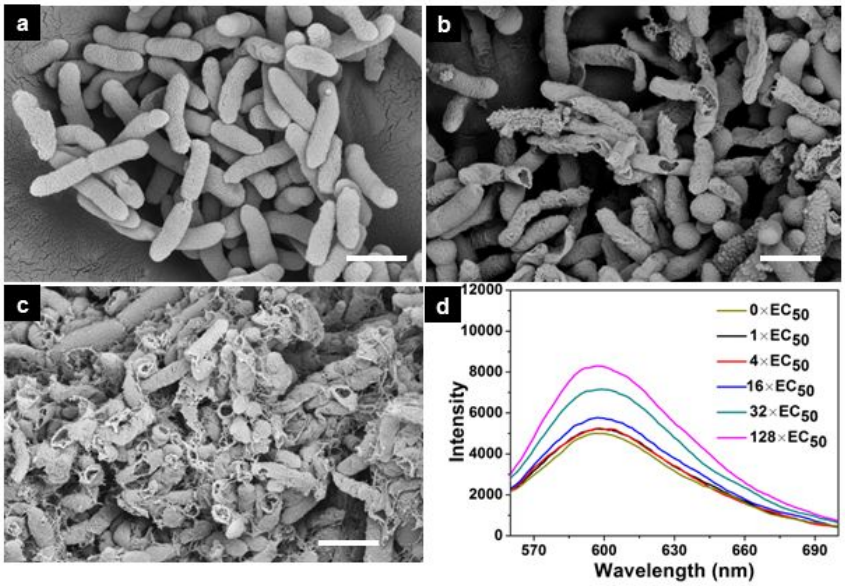

684

685

686 **Graphic for Table of Contents**

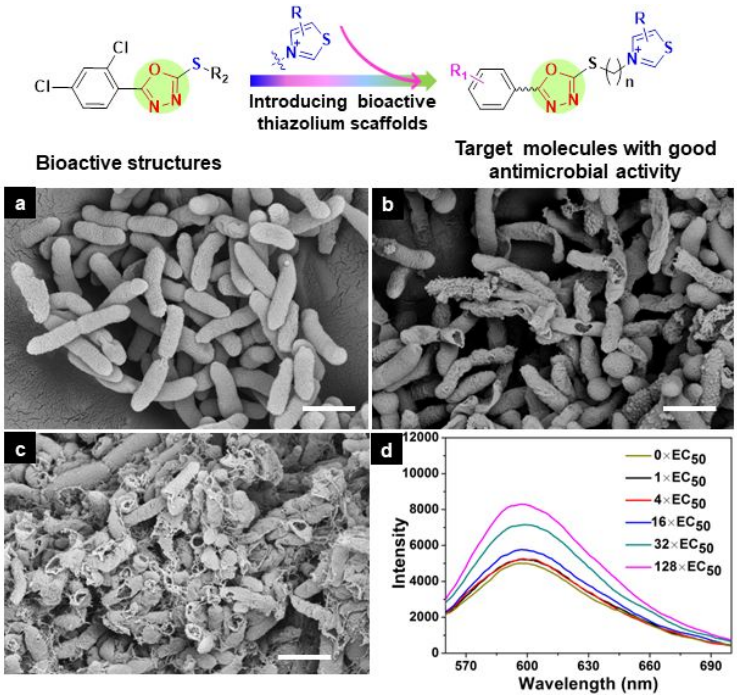

687